Dependence of Invadopodia Function on Collagen Fiber Spacing and Cross-Linking: Computational Modeling and Experimental Evidence

Heiko Enderling,* Nelson R. Alexander,† Emily S. Clark,† Kevin M. Branch,† Lourdes Estrada,† Cornelia Crooke,‡ Jérôme Jourquin,† Nichole Lobdell,† Muhammad H. Zaman,§ Scott A. Guelcher,¶ Alexander R. A. Anderson,‖ and Alissa M. Weaver†

*Center of Cancer Systems Biology, Caritas St. Elizabeth's Medical Center, Tufts University School of Medicine, Boston, Massachusetts 02135; †Department of Cancer Biology, and ‡Department of Biochemistry, Vanderbilt University, Nashville, Tennessee 37232; §Department of Biomedical Engineering, University of Texas, Austin, Texas 78712-0238; ¶Department of Chemical Engineering, Vanderbilt University, Nashville, Tennessee 37235; and ‖Division of Mathematics, University of Dundee, Dundee DD14HN, United Kingdom

ABSTRACT Invadopodia are subcellular organelles thought to be critical for extracellular matrix (ECM) degradation and the movement of cells through tissues. Here we examine invadopodia generation, turnover, and function in relation to two structural aspects of the ECM substrates they degrade: cross-linking and fiber density. We set up a cellular automaton computational model that simulates ECM penetration and degradation by invadopodia. Experiments with denatured collagen (gelatin) were used to calibrate the model and demonstrate the inhibitory effect of ECM cross-linking on invadopodia degradation and penetration. Incorporation of dynamic invadopodia behavior into the model amplified the effect of cross-linking on ECM degradation, and was used to model feedback from the ECM. When the model was parameterized with spatial fibrillar dimensions that closely matched the organization, in real life, of native ECM collagen into triple-helical monomers, microfibrils, and macrofibrils, little or no inhibition of invadopodia penetration was observed in simulations of sparse collagen gels, no matter how high the degree of cross-linking. Experimental validation, using live-cell imaging of invadopodia in cells plated on cross-linked gelatin, was consistent with simulations in which ECM cross-linking led to higher rates of both invadopodia retraction and formation. Analyses of invadopodia function from cells plated on cross-linked gelatin and collagen gels under standard concentrations were consistent with simulation results in which sparse collagen gels provided a weak barrier to invadopodia. These results suggest that the organization of collagen, as it may occur in stroma or in vitro collagen gels, forms gaps large enough so as to have little impact on invadopodia penetration/degradation. By contrast, dense ECM, such as gelatin or possibly basement membranes, is an effective obstacle to invadopodia penetration and degradation, particularly when cross-linked. These results provide a novel framework for further studies on ECM structure and modifications that affect invadopodia and tissue invasion by cells.

INTRODUCTION

The cellular machinery used by cancer cells to degrade extracellular matrices is thought to be invadopodia, i.e., slender, actin-rich protrusions with associated extracellular proteases (1,2). Understanding the mechanisms that lead to functional invadopodia is a subject of intense study; key cellular processes include signal generation, actin polymerization, extracellular matrix (ECM) degradation, and membrane protrusion (2). It is thought that cellular growth factor and adhesion signals combine to induce branched actin assembly and membrane protrusion in the form of invadopodia. The secretion of proteases is a linked process that is likely essential to promote protrusion into the matrix through degradation of the ECM and removal of space constraints.

Despite intimate interaction of invadopodia with the ECM, very little is known about the role, if any, of ECM characteristics in regulating invadopodia function. Artym et al. (3) used a live-cell imaging approach to demonstrate that ECM degradation rapidly follows the recruitment of the actin assembly molecule cortactin, suggesting that matrix degradation is a secondary but linked step. However, both that and another study provided evidence that the inhibition of ECM degradation with matrix metalloproteinase (MMP) inhibitors leads to decreased numbers of invadopodia actin puncta, suggesting that the degradation of the ECM may provide positive feedback to invadopodia through unknown mechanisms (3,4). Burgstaller and Gimona reported that structures related to invadopodia, i.e., podosomes, could not degrade cross-linked ECM matrices (5). However, this observation was only mentioned in the text, without showing specific data. Thus, the regulation of invadopodia dynamics and function by the ECM occurs, but is poorly understood and likely to be complex.

Cross-linking of basement membranes and other extracellular matrices is an important modification that is thought to inhibit cell invasion and tissue remodeling (6–9). In vivo, enzymes such transglutaminase 2 (TG2) and lysyl oxidase cross-link a variety of ECM substrates, including fibronectin, collagen, fibrinogen, nidogen, osteonectin, osteopontin, vitronectin, and elastin (10–12). This modification is thought to promote assembly and provide mechanical stability to the

Submitted March 9, 2008, and accepted for publication May 9, 2008.

Heiko Enderling and Nelson R. Alexander contributed equally to this work.

Address reprint requests to Alissa M. Weaver, Department of Cancer Biology, Vanderbilt University, Nashville, TN 37232. E-mail: alissa.weaver@vanderbilt.edu.

Nelson R. Alexander's present address is Ventana Medical Systems, Inc., Tucson, AZ 85755.

Editor: Alexander Mogilner.

0006-3495/08/09/2203/16 $2.00

doi: 10.1529/biophysj.108.133199

ECM. In cancer, TG2 was implicated in inhibiting primary tumor growth, tumor invasion, and metastasis (8,13,14). Likewise, lysyl oxidase is frequently downregulated in primary tumors, and may act as a tumor suppressor (15–17). However, depending on the context, TG2 and lysyl oxidase may also promote tumor aggressiveness through such mechanisms as the promotion of fibronectin assembly and signaling (17–19). In vitro, the effect of cross-linking is frequently ignored, because such substrates as pepsinized collagen I (e.g., most type I collagen preparations not derived from rat tail) gels and matrigel lack significant cross-links between molecules, and primarily rely on noncovalent interactions to provide gelling properties (6,7). In this study, we investigate the specific role of ECM cross-linking on invadopodia function in gelatin and collagen matrices.

The formation of invadopodia is a complex process, governed by many variables. Computational and mathematical models are valuable, if not essential, tools to investigate complex processes in biology and other disciplines. Modeling creates a theoretical framework for describing biologic systems with a minimum number of rules and equations that capture the essence of the process. Individual model elements can then be altered to identify key governing variables and generate hypotheses that can guide experimentation. Modeling has proven useful in cell motility (20–23), but surprisingly, there have been no models of invadopodia function.

In this study, we report on the development of a computational cellular automata model of the interaction of invadopodia with ECM fibers, focusing on the effect of fiber cross-linking. We interactively performed experiments to aid in both model design and testing. In fixed and live-cell experimental studies on dense denatured collagen (gelatin) substrates, we found that cross-linking inhibits ECM degradation and penetration by invadopodia, and reduces invadopodia lifetimes. The model was used to investigate the interplay between invadopodia dynamics and ECM organization on invadopodia function in cross-linked ECM. Our results suggest that dense ECM substrates (such as gelatin) or basement membranes provide efficient substrates for proteolysis and strong barriers to individual invadopodium protrusion. Conversely, sparse collagen substrates, such as those that may approximate loose connective tissue, provide a weak barrier to invadopodia, and may only occasionally serve to stabilize dynamic invadopodia protrusions for the induction of ECM degradation.

EXPERIMENTAL PROCEDURES

Cell culture and ECM degradation assay

Invasive breast cancer cell line MCF10A-CA1d (24) was obtained from Dr. Fred Miller (Karmanos Institute, Detroit, MI) and cultured in Dulbecco's Modified Eagle Medium (DMEM) supplemented with 10% fetal bovine serum (FBS) at 37°C, with constant humidity. For the ECM degradation assay, cells were cultured at a 1:1 ratio of DMEM:RPMI-1640 with 5% NuSerum (Gibco, Carlsbad, CA), 10% FBS, and 20 ng/mL epidermal growth factor (EGF).

To prepare ECM substrates for invadopodia assays, MatTek (MatTek Corp., Ashland, MA) culture plates were coated with a thin layer of fluorescein isothiocyanate (FITC)-conjugated gelatin (25 mg/mL; gelatin from Polysciences, Inc., Warrington, PA; FITC-labeled as previously described (25)), or 1 mg/mL FITC-conjugated type I collagen (Sigma, St. Louis, MO), and briefly allowed to dry. Dishes used in confocal microscopy were coated with two layers of FITC-conjugated ECM, yielding gels of $\sim 2\ \mu$m in height. Phosphate-buffered saline (PBS) containing different concentrations of glutaraldehyde (Polysciences, Inc.) was added to gelatin-coated or type I collagen-coated plates for 15 min on ice, and then for an additional 30 min at room temperature. Plates were washed with PBS and treated with 1% $NaBH_4$ for 3 min at room temperature. Plates were incubated in culture media for 30 min before cell plating. For experiments, cells were plated at 5000 cells/cm^2. Cells were cultured for 20 hr, at which point they were fixed with 4% paraformaldehyde for 20 min at 37°C, washed with PBS, and permeabilized with 0.1% Triton X-100 for 5 min at room temperature. Cells were blocked in 3% bovine serum albumin (BSA) for 1 hr at room temperature, and rhodamine-labeled phalloidin (Molecular Probes, Carlsbad, CA) (3 nM in PBS with 3% BSA, 1 hr at room temperature) was used to stain actin filaments (F-actin). Wide-field fluorescent images were captured on a Nikon Eclipse TE2000-E microscope with a 40× Plan Fluor oil immersion objective lens. Confocal images were obtained on a Zeiss LSM 510, using a Plan APO 63× 1.4 NA oil immersion objective lens. The Z-section images were captured by scanning at 8 s per 0.05-μm focal section, using the appropriate pinhole setting to yield a 1-Airy disk diameter unit.

Electron microscopy

Cells were cultured overnight on transwells (6.5-mm, 8.0-μm pore size; Fisher Scientific, Pittsburgh, PA) coated with gelatin. The transwell membrane was removed, fixed in 2.5% glutaraldehyde in 0.1 M cacodylate buffer, stained in 1% osmium tetraoxide, dehydrated in successive alcohol incubations, and embedded in Spurr's resin overnight. Sections (100 nm) were cut, with the cells remaining on the transwells to ensure proper orientation. Electron microscopy was performed using a Philips CM-12 functioning at 80 keV.

Rheometry

To determine the storage modulus of gelatin treated with various concentrations of glutaraldehyde, we performed rheometry on an AR-G2 rheometer (TA Instruments, New Castle, DE) at 37°C, using a 20-mm circular head. Gels were compressed between a heated Peltier plate and a 20-mm upper plate, and were subjected to an oscillating shear strain that was in the linear range determined by strain sweep tests. The storage modulus was measured as a function of frequency, which varied from 0.1–10 Hz.

Live-cell imaging

For the expression of GFP-ARPC1 (the p41 subunit of the Arp2/3 complex) in MCF10A-CA1d cells, the coding sequence of ARPC1 fused with green fluorescent protein (GFP) (a kind gift of Theresia Stradal, German Research Centre for Biotechnology, Braunschweig, Germany) was cloned into LZRS-Neo retroviral expression vector (26). Phoenix 293 packaging cells (from Garry Nolan, Stanford University, Stanford, CA) were maintained in DMEM supplemented with 10% heat-inactivated bovine growth serum (Hyclone, Logan, UT). Phoenix 293 cell transfection, viral harvest, and target-cell transduction were performed as previously described (26). Cells were selected with 4 μg/mL puromycin or 600 μg/mL G418 for the expression of pRS or LZRS-Neo, respectively.

The GFP-ARPC1-expressing MCF10A-CA1d cells were cultured overnight, using our standard ECM degradation assay technique, except that the 2.5% gelatin was conjugated to Texas red, instead of FITC. For image acquisition, cells were changed into phenol red-free L15 media (containing 5% NuSerum, 10% FBS, and 20 ng/mL EGF). Cells were transferred to a tem-

perature-controlled (37°C) humidified chamber surrounding a Nikon Eclipse TE2000-E microscope. Images were captured every minute for 2 h with a 40× Plan Fluor oil immersion objective lens, using MetaMorph software (Molecular Devices, Sunnyvale, CA).

Image analysis, quantification, and statistics

The images that were used to determine degradation area and invadopodia number were analyzed using Metamorph software. Invadopodia were defined in two ways: 1), functional invadopodia, i.e., actin puncta that colocalized with areas of ECM degradation; and 2), total invadopodia, i.e., any focal F-actin-positive or GFP-ARPC1-positive structures that were circular, whether or not they were associated with ECM degradation. These two types of invadopodia were manually counted from images and reported as invadopodia per cell. Cell area was determined by manually tracing the outline of cells, using the F-actin staining, to define the footprint of the cell, followed by calculation using the region-of-interest tool in Metamorph software. Degradation area was determined by performing an inclusive threshold of the FITC channel to include the dark, degraded areas. Then the region-of-interest tool was used to calculate the threshold area. The degradation area was then divided by the cell area to obtain a quantification of degradation area/cell area for plots of ECM degradation. Invadopodium penetration depth was determined from confocal Z-stacks, using a Zeiss LSM Image Browser. The deepest point of the invadopodium was standardized as the point where the half-maximum intensity of the rhodamine-phalloidin signal occurred, and was determined by a line profile drawn through the middle of the invadopodium. The top of the fibronectin matrix was standardized as 2 SDs above the average noise signal from the FITC-fibronectin. This noise was determined by a line profile drawn in the Z-stack well above the invadopodium in the cell. The penetration depth of the invadopodium was calculated as the distance between the bottom tip of the invadopodium and the top of the fibronectin matrix, as determined above. Statistical analyses of biological data were performed using Student's *t*-test in GraphPad Prism4 software, with statistical significance set at $p < 0.05$. All data are reported as mean ± SE.

RESULTS

Invadopodia are slender protrusions (Fig. 1) that penetrate and degrade ECM, and are thought to be the invasive organelles of cancer cells. The goal of our study was to build a model of invadopodia-ECM interactions that could be used interactively with experimentation to better understand how different ECM characteristics regulate invadopodia formation and function. We initially built a simple model (not shown) in which the ECM was represented phenomenologically as a ''harsh'' barrier that influenced invadopodial protrusion. However, it became immediately clear that the incorporation of ECM physicochemical characteristics was necessary to provide constraints and realism to this initial model. There is a dearth of published information on the effect of ECM parameters on invadopodia function. Therefore, we performed empirical determinations from which ECM cross-linking emerged as a likely ''harsh'' inhibitory factor for invadopodia function.

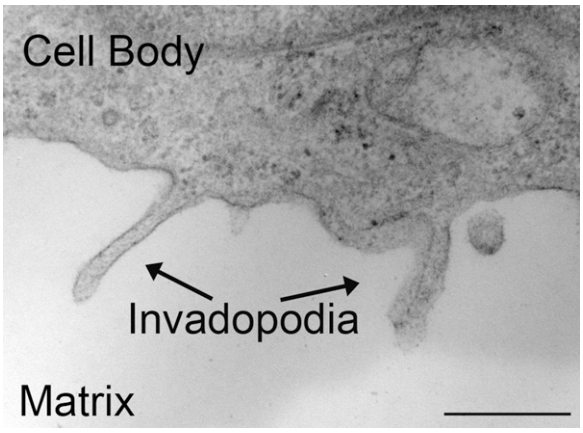

FIGURE 1 Electron-micrograph image of cancer-cell invadopodia. Ultrathin vertical-section electron micrograph of an SCC-61 oral squamous carcinoma cell, attached to fibronectin, reveals multiple invadopodia protruding into the underlying matrix. Scale bar = 500 nm.

Pilot experimental data for model design

The effect of ECM cross-linking on invadopodia penetration was experimentally tested with the commonly used substrate, FITC-gelatin (25). We altered the content of ECM cross-links by treating FITC-gelatin with glutaraldehyde, a chemical that covalently cross-links lysine amino acids and is used to cross-link gelatin in these assays. Consistent with glutaraldehyde-induced cross-linking, an increase in gelatin rigidity was observed by rheological measurements of samples treated with increasing concentrations of glutaraldehyde (see Fig. S1 in Supplementary Material, Data S1) (27). To determine the depth of invadopodia penetration, we used confocal microscopy to measure the length of individual invadopodia in cells that were plated on 25 mg/mL FITC-gelatin that was cross-linked with either a low (0.1%) or high (2.5%) concentration of glutaraldehyde in buffer. A standard concentration of glutaraldehyde that is typically used in these assays is 0.5% (25). As shown in Fig. 2 *D*, invadopodia from cells cultured on gelatin substrates that are weakly cross-linked protrude an average of 0.72 ± 0.03 μm into the ECM. Conversely, cells cultured on gelatin substrates that are extensively cross-linked have a 26% reduction in the depth of invadopodia protrusion (0.53 ± 0.04 μm, Fig. 2).

We also determined whether cross-linking affects the number and ECM-degrading capacity of invadopodia by fixing and staining cells that were cultured overnight on FITC-gelatin substrates cross-linked with various concentrations of glutaraldehyde. Interestingly, we found that cells plated on more heavily cross-linked substrates exhibit less ECM degradation area/cell area and fewer functional ECM-degrading invadopodia (decreases of 79% and 47%, respectively, in cells plated on 2.5% glutaraldehyde treated-substrates, compared with those cross-linked with 0.1% glutaraldehyde), but the same number of total invadopodia actin puncta (Fig. 3). Thus, the major impact of cross-linking appears to be the inhibition of ECM degradation by invadopodia, and not an effect on the overall number of invadopodia.

Development of cellular automaton model

Based on these data, we designed rules for a cellular automaton model. We assumed that the cell sits on top of a grid,

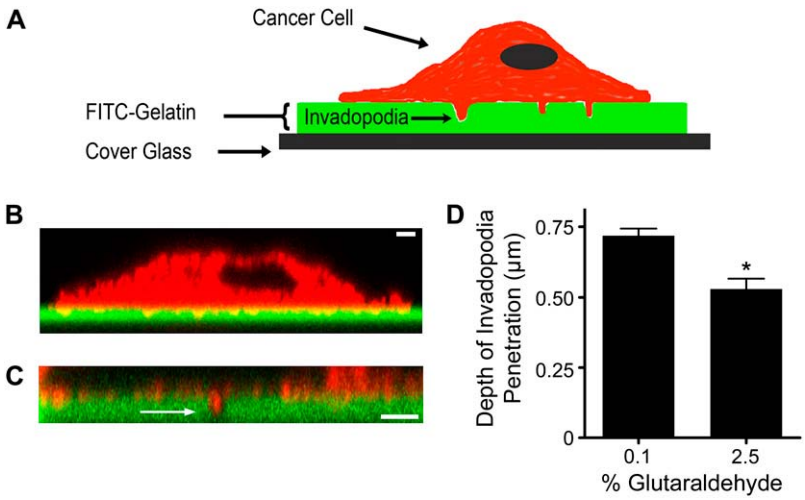

FIGURE 2 The depth of invadopodia penetration is regulated by ECM cross-linking. (*A*) For the visualization of invadopodia, cancer cells were allowed to adhere to cover glass that was coated with FITC-conjugated gelatin. Cancer cells developed invadopodia that degraded the surrounding ECM, and penetrated into the FITC-gelatin. (*B*) Confocal Z-section of CA1D breast-cancer cell stained with rhodamine phalloidin, to identify actin filaments (*red*) attached to FITC-gelatin (*green*), with multiple invadopodia protruding into the underlying ECM. Scale bar = 2 μm. (*C*) Representative Z-section, to quantify invadopodia penetration depth, shows a close-up of a CA1D invadopodium (*arrow*) that degraded and protruded into the FITC-gelatin. Scale bar = 2 μm. (*D*) Quantification of invadopodia penetration depth of CA1D cells cultured on FITC-gelatin gels that were cross-linked with 0.1% or 2.5% glutaraldehyde buffer. Data are reported as mean ± SE, and are from three independent experiments. $*p < 0.05$.

with several invadopodia growing and penetrating into a two-dimensional (2D) ECM (Fig. 4 *B*). We assumed that one time unit in our simulations corresponds to the time it takes an invadopodium to migrate and invade one space unit in a perfectly favorable ECM. The penetration and degradation of the ECM domain by the invadopodium is then governed by probabilistic rules (Table 1) that take into account ECM-invadopodia interactions.

To create a realistic model that could be experimentally tested, we included several important features. First, we matched the computational ECM domain as closely as possible to the experimental system by using biologically relevant length scales, including gelatin length and width, invadopodium width, and number of ECM molecules. Second, we incorporated assumptions based on our experimental data into the rules, such that the cross-linking of ECM fibers carries a penalty in terms of both the penetration and degradation of the ECM. Fibers themselves do not carry any direct penalty for invadopodium penetration; however, the number of cross-links in a given ECM domain depends on the number of fibers. These rules provide the foundation for simulations that can be used to test different scenarios. Because we matched certain critical parameters such as fiber number and invadopodium width, the model can be used interactively with experimentation.

Invadopodia and ECM domain dimensions

Taking physiologic length scales into account, the size of the ECM domain is set at 2000 × 1000 pixels, which corresponds

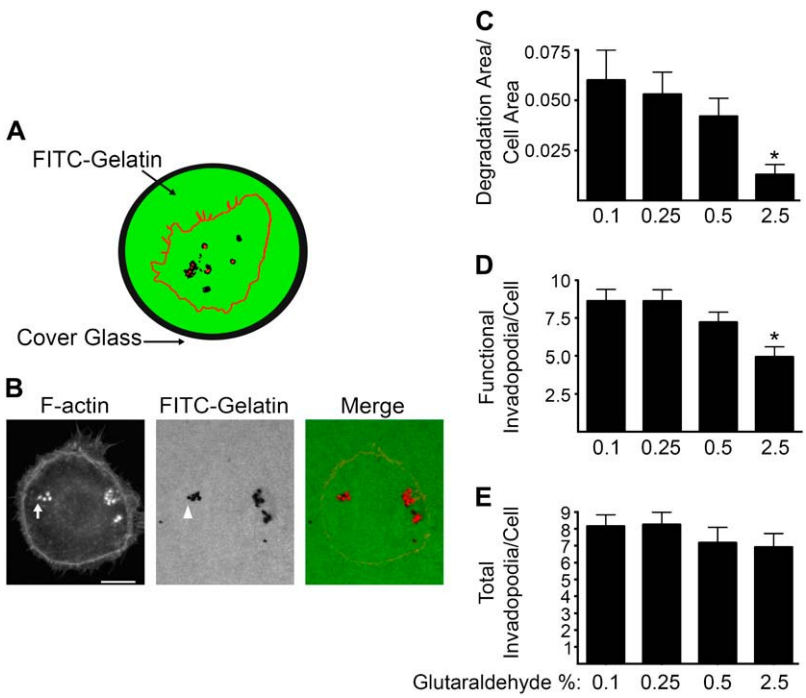

FIGURE 3 Invadopodia-associated ECM degradation is regulated by cross-linking. (*A*) Depiction of a typical image from wide-field microscopy of a rhodamine-phalloidin-stained cell (rhodamine-phalloidin stains actin filaments *red*), cultured for 18 h on FITC-gelatin (*green*). Functional invadopodia degraded the FITC-gelatin, leaving black areas with no FITC fluorescence. Invadopodia were defined as punctate spots of F-actin staining localized to areas of degradation, and appear as red spots against a black background. (*B*) Representative wide-field image of a CA1D cell cultured on gelatin that was cross-linked with 0.1% glutaraldehdye buffer. Arrow indicates a cluster of four distinct invadopodia. Arrowhead indicates area of FITC-gelatin degradation from the invadopodia (*arrow*). This clustering of invadopodia was typical in these cells. Scale bar = 10 μm. (*C*) Quantification of total area of FITC-gelatin degradation per cell, from experiments using CA1D cells cultured on FITC-gelatin gels that were cross-linked with different percentages of glutaraldehyde buffer. (*D*) Quantification of number of functional invadopodia (actin puncta associated with FITC-gelatin degradation) per cell. (*E*) Quantification of total number of invadopodia (all actin puncta, regardless of associated degraded ECM) per cell. Data are reported as mean ± SE, and are from three independent experiments. $*p < 0.05$, compared with 0.1% glutaraldehyde condition.

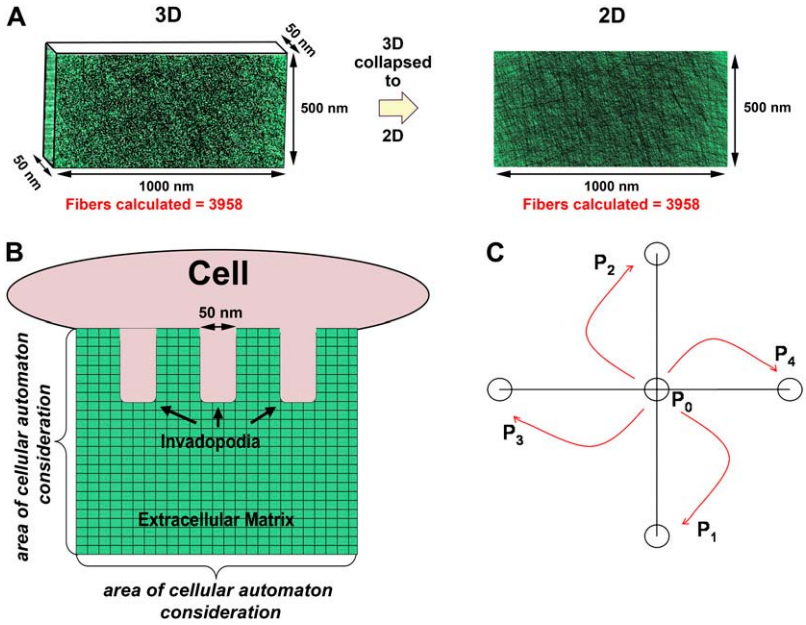

FIGURE 4 Schematic of cellular automaton model. (*A*) Calculation of fiber number in the ECM domain. Fiber number was calculated from the number of single-stranded gelatin molecules that were contained in a 50-nm-thick slice of 2.5% gelatin, as might be experienced by an invadopodium in experiments. That fiber number (3958) was then used in 2D simulations. (*B*) Scale of computational model. We assumed that a cell sat on top of the extracellular matrix, and in simulations we considered only the area of ECM in which the invadopodia protruded beneath the cell. (*C*) Schematic of the probability distribution of invadopodia moving and protruding into the computational ECM. P_1 is the probability of downward movement into the gel. P_2 is the probability of upward movement, toward the cell-ECM interface. P_3 and P_4 are the probabilities of moving left or right, respectively. P_0 is the probability of staying stationary.

to 1 μm wide by 0.5 μm high; thus, 1 pixel = 0.5 nm $\times$ 0.5 nm. The width of simulated invadopodia is set at 50 nm (100 pixels), based on measurements from electron micrographs of invadopodia by our laboratory (Fig. 1) and others (28). The size of gelatin molecules in the model was set at 300 nm long and 0.5 nm in diameter. These numbers were based on the assumption that gelatin consists of denatured but undegraded single-stranded type I collagen, which should approximate the high Bloom gelatin used in our experimental protocol. Triple-helix collagen monomers have dimensions of ~300 nm in length and 1.5 nm in diameter (29–32). Thus, the dimensions of gelatin in the model are set at one third the width and the same length as triple-helical collagen monomers. Although gelatin is a heterogeneous mixture, there is thought to be little higher-order structure (30,32), and for simplicity, we assumed that the molecules adopt a uniform single-stranded, linear conformation. This assumption may underestimate the number of cross-links that a gelatin molecule can have, because it prevents any intramolecular cross-linking of random coil structure. However, it allows easy comparison with native collagen monomers and fibrils that are known to be linear, and avoids the need to guess the secondary structure of gelatin, which is unknown.

To simulate the number of ECM molecules that an invadopodium would experience during protrusion, we took the number of ECM molecules that would be contained in a three-dimensional (3D) ''slice'' of ECM in which the depth is 50 nm (the diameter of an invadopodium), and the width and height are the size of the simulated ECM domain (1 μm $\times$ 0.5 μm) (Fig. 4 *A*). Thus, we use Avogadro's number to calculate that the number of gelatin molecules/fibers contained in a 25 mg/mL gelatin gel with dimensions of 1 $\times$ 0.5 $\times$ 0.05 μm^3 is 3958. This number of gelatin molecules is then used in 2D simulations to test the interactions between invadopodia and the ECM (Fig. 4). Because fibers have no preferred direction, their initial direction is randomly distributed over the unit sphere. For each fiber, we randomly initiated a fiber endpoint $P(x,y)$, and used standard computer-graphic line-segment algorithms to map the fiber with the randomly chosen direction onto our discrete lattice. Each simulation, therefore, had a slightly different random distribution of ECM. Thus, for each condition, many simulations were run, and the results plotted as mean $\pm$ SE.

Movement probabilities, ECM degradation, and cross-linking penalty

We assumed in the model that there are cellular signals that allow invadopodia formation and protrusion, e.g., through growth factor or integrin-based adhesion signals. Based on this assumption, we initiated each simulation with four invadopodia at the top of an ECM domain. The primary protrusive direction of invadopodia during penetration into the ECM can be seen in electron micrographs to be downward, away from the ventral surface of the cell body (Fig. 1) (28). Thus, with the ventral surface of the cell adherent to the ECM in our model (Fig. 4 *B*), we defined ''downward'' as the preferred protrusive direction. To account for biological variation, we assumed that an invadopodium can grow in four orthogonal directions as well as remain stationary, and we associated those directions with the following probabilities of p_1 downward, p_2 upward, p_3 left, p_4 right, and p_0 with no movement (Fig. 4 *C*). We assumed that $p_1 > p_{3,4} > p_{0,2}$ to reproduce the directionality of invadopodium protrusion that we observed in electron micrographs from cancer cells (Fig. 1). As a baseline set of parameters for the simulation of invadopodial protrusion in a uniform matrix, we therefore took $p_1 = 0.5$, $p_3 = p_4 = 0.24$, $p_0 = p_2 = 0.01$, with the sum

TABLE 1 Rules used in simulations

	Figs. 4 and 5 (baseline rules affecting penetration and degradation):
ECM characteristics	1. ECM is treated as degradable fibers; intersections of fibers can be cross-linked. 2. Gelatin is modeled as denatured single-stranded collagen, 300 nm long × 0.5 nm wide.
Invadopodia movement	1. Invadopodia move according to baseline probabilities that are then modified by interactions with cross-linked ECM, according to the cross-linking penalty. 2. Invadopodia move equally well into free space and through uncross-linked fiber meshwork, i.e., there is no impedance of movement by fibers unless they are cross-linked. 3. Penetration and degradation of ECM occur simultaneously.
Penalties	1. A cross-linking penalty $\chi = e^{-[\beta * cl/\delta]}$ (where $\beta = 2$ is a constant, cl = number of cross-links encountered by an invadopodia in all directions, and δ = the moving surface of invadopodia that experiences fiber cross-links) redistributes probabilities of invadopodia movement. 2. Let $\overline{p_i} = \chi p_i$ be the scaled moving probabilities for all p_i. Then $\varphi_i = p_i - \overline{p_i}$ is the difference between original and scaled moving probabilities. The new moving probabilities $\overline{\overline{p_i}}$ are calculated using the scaled probabilities $\overline{p_i}$ plus the respective share of the probabilities that need to be redistributed $\phi_{j\neq i}$, as follows: $$\overbrace{\overline{\overline{p_i}}}^{\text{new probability}} = \overbrace{\overline{p_i}}^{\text{scaled probability}} + \sum_{j\neq i} \overbrace{\varphi_j}^{\text{to be redistributed}} \left(\overbrace{\overline{p_i} / \sum_{k\neq j} \overline{p_k}}^{\text{ratio within all receiving probabilities}} \right)$$ i.e., new p_1 = scaled p_1 + respective probabilities from scaled p_2, p_3, and p_4.
	Figs. 6 and 7 (regulation of invadopodia dynamics):
Retraction	Invadopodia become retracted if they have not degraded any fibers/cross-links for $\psi = 15$ consecutive time steps.
Formation	Default background initiation of new invadopodia with a probability of $\zeta \times 1/1500$ (once every 1500 time steps when $\zeta = 1$).
Negative feedback	If any invadopodia are retracted, background formation will be inhibited with $\zeta < 1$ (i.e., a longer wait until next one is initialized; with each retraction, the rate of formation is decreased). rate of formation is decreased).
Positive feedback	If any invadopodia are retracted, background formation will be promoted with $\zeta > 1$ (i.e., initialized faster; with each retraction, the rate of formation is decreased).
	Fig. 9 (model implementation with diverse ECM domains):
ECM characteristics	1. Gelatin was modeled as denatured, single-stranded collagen, 300 nm long × 0.5 nm wide. 2. Collagen monomers were modeled as a triple helix, 300 nm long × 1.5 nm wide. 3. Collagen microfibrils were modeled as 15 α-chains per microfibril, 300 nm long × 4 nm wide.
	Simulations were run with rules from Fig. 5 or Fig. 7, as indicated.

of all probabilities = 1 (Fig. 4 *C*). Thus, the invadopodium follows a biased random walk, with the highest likelihood of migrating downward, and the lowest chance of remaining stationary or migrating upward. We assumed that fiber degradation occurs instantaneously when invadopodia encounter fibers, and hence fiber pixels are voided immediately. Because we modeled the invadopodial tip as blunt-ended, advancement in the p_1 direction leads to uniform degradation at the very tip. Modeling a more rounded end (e.g., similar to the invadopodia in Fig. 1, *left*) would lead to slightly more focused and less efficient degradation of the domain as the invadopodium advances in a given direction. We hypothesized that in a nonuniform ECM, the direction of invadopodium protrusion would be affected by the physical interaction between the invadopodium and the ECM. Therefore, in the model, the probabilities of invadopodium movement were modified by physical ECM parameters (below). For this initial model, we focused on cross-linking, but in future developments, other ECM characteristics could be used to alter the movement probabilities.

To simulate fiber cross-linking, we introduced a certain ratio of cross-links when two or more fibers intersect. Fibers themselves do not carry any direct penalty for invadopodium penetration. However, the number of cross-links in a given ECM domain depends on the number of fibers. Fig. 5 *A* shows a schematic of 12 fibers in a random organization with 13 intersections between them (*red circles*), and cross-linking ratios of 50% and 100% (*blue dots* indicate cross-links). To model the inhibition of ECM degradation and penetration that occurs with ECM cross-linking (Figs. 2 and 3), we designated a cross-linking penalty in which fiber cross-links that are encountered by the moving surface of the invadopodium modify the baseline movement probabilities. The cross-linking penalty was defined as $\chi = e^{-[\beta * cl/\delta]}$, where cl = the number of cross-links encountered by the invadopodium in each direction, δ = the moving surface of the invadopodium that experiences fiber cross-links, and β is a constant used to calibrate the penalty. Then, χ is used to recalculate the scaled movement probabilities, $\overline{p_i}$, for each movement direction p_i, where $\overline{p_i} = \chi p_i$. The probabilities that need to be redistributed to other directions are then $\varphi_i = p_i - \overline{p_i}$, which is the difference between the original and scaled moving probabilities. The new moving probabilities $\overline{\overline{p_i}}$ are then calculated, using the scaled probabilities $\overline{p_i}$ plus the

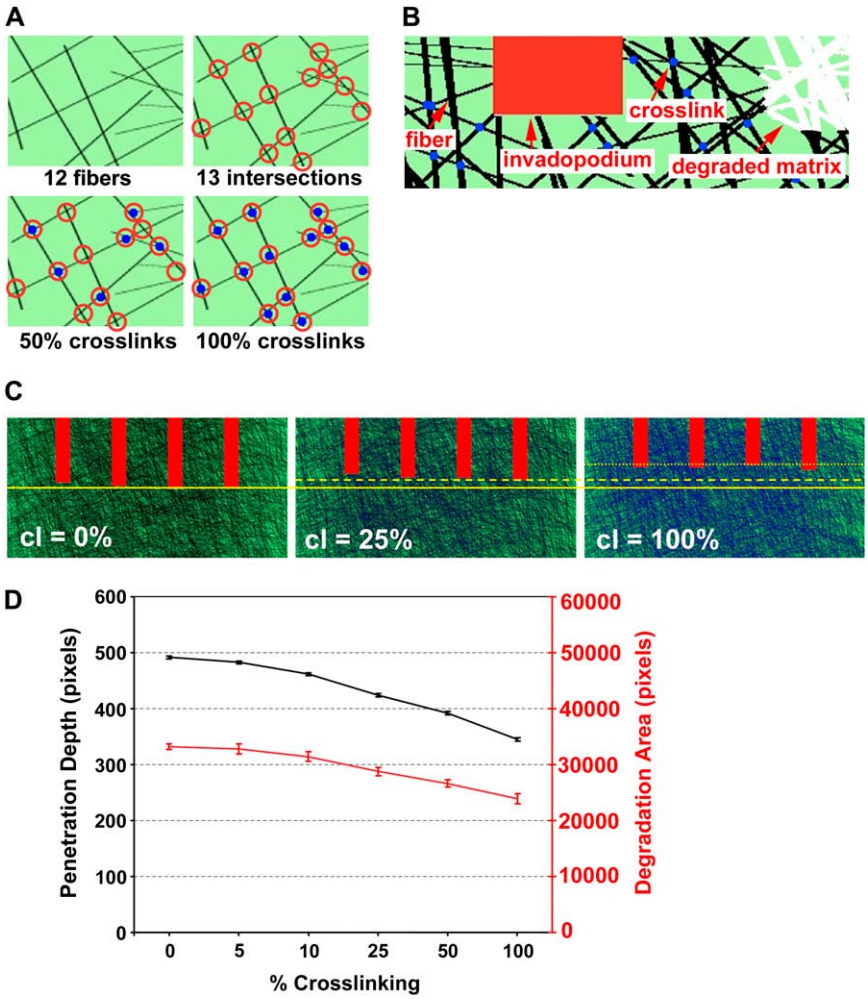

FIGURE 5 Invadopodia penetration in simulated gelatin: effect of a penalty for ECM cross-linking. (*A*) Enlarged view of a simulated ECM domain that contains 12 fibers with 13 intersections (*red circles*). Cross-links (*blue dots*) at intersecting fibers are shown for 50% and 100% cross-link ratios, respectively. (*B*) An invadopodium (*red*) invades a matrix with several cross-linked (*blue*) and unlinked fibers (*black*). Degraded ECM fibers (*white*) are also shown. The contents of *A* and *B* are not to scale. (*C*) Sample screen shots from simulations of invadopodia protruding into an ECM domain with 3958 fibers and cross-link ratios $cl = 0\%$, 25%, and 100% at $t = 1000$ time steps. (*D*) Penetration depth (*black*) and ECM degradation (*red*) for invadopodia protruding into gelatin domains with different cross-linking ratios. Simulations were run for 1000 time steps for each cross-linking variable. Shown is the mean ± SE from 40 invadopodia for each condition. See also Movie S1.

respective share of the probabilities that need to be redistributed, $\phi_{j\neq i}$, as follows:

$$\overbrace{\overline{\overline{p_i}}}^{\text{new probability}} = \overbrace{\overline{p_i}}^{\text{scaled probability}} + \sum_{j\neq i} \overbrace{\varphi_j}^{\text{to be redistributed}} \left(\overbrace{\overline{p_i} / \sum_{k\neq j} \overline{p_k}}^{\text{ratio within all receiving probabilities}} \right)$$

e.g., a new p_1 = scaled p_1 + respective probabilities from scaled p_2, p_3, and p_4.

An example of a single invadopodium penetrating an ECM with cross-linked fibers is shown in Fig. 5 *B*. To analyze the impact of fiber cross-linking on invadopodium formation in our model, we ran simulations for 1000 time steps with different cross-linking ratios, and compared the average penetration depths of 40 invadopodia. In these simulations, the ECM consisted of 3958 ECM fibers with cross-linking ratios of 0%, 5%, 10%, 25%, 50%, and 100%. For these and subsequent simulations, we set $\beta = 2$, which leads to a decrease in both penetration depth and degradation area of ~30% between the 0% and 100% cross-linking conditions (Fig. 5, *C* and *D*, and Movie S1). The value of β was estimated to match the decrease in penetration depth from Fig. 2 of ~ 26% between the 0.1% and 2.5% glutaraldehyde conditions. Based on the calculations of others using 0-5% glutaraldehyde on gelatin (27) and our storage modulus measurements (see Fig. S1 in Data S1), we estimated that the cross-linking was likely to be close to saturating at this percentage. However, if that is not the case, then we underestimated our cross-linking penalty, and β should be higher, to match our conditions. The effect of altering the cross-linking penalty via β is shown in Fig. S2 *A* in Data S1. The magnitude of the outcomes, but not the overall trend, changes, i.e., increased cross-linking leads to decreased ECM degradation and invadopodium penetration into the ECM. Similarly, although the trend is the same, altering the fiber number has a large effect on penetration and degradation at different cross-link ratios because of the dependence of cross-link density on the number of fibers that can intersect each other (see Fig. S2 *B* in Data S1).

Incorporation of invadopodia dynamics and feedback

One of the goals of this study was to build a simple but realistic model that can be used to investigate the regulation of invadopodia function by different ECM attributes. In real cells, invadopodia are constantly forming and disappearing,

with lifetimes varying from <20 min to >240 min (33,34). Disappearance of the structural invadopodial actin core (33,34) presumably leads to the retraction of invadopodia protrusions, similar to other actin-based protrusions. Although little is known about ECM-invadopodia interactions, it seems likely that feedback from the matrix may constitute at least one factor regulating invadopodia dynamics, especially given the concentration of signaling and adhesion molecules in invadopodia (2), the observed negative effect of MMP inhibitors on invadopodia puncta (3,4), and the frequent clustering of invadopodia in distinct subcellular locations (Fig. 3 *B*). We therefore incorporated invadopodia dynamics into the model, and examined the impact of cross-linking on the retraction and formation of invadopodia.

To model retraction, we first tried increasing the baseline probability of upward movement to determine whether we could observe spontaneous retraction behavior that would be enhanced by cross-linking. However, higher upward movement probabilities led either to an inability to produce significant protrusion of invadopodia into the ECM domain, or to a prolongation of the simulation times required to observe the same behavior (results not shown). Therefore, we needed to introduce a specific rule governing the retraction of already successfully protruding invadopodia.

Several biologic factors might lead to invadopodia retraction, including: 1) loss of feed-forward signals from growth factors or integrin-ECM signaling; 2) a specific negative signal from the microenvironment; and 3) loss of adhesion to the ECM, as might occur in highly cross-linked ECM with inaccessible MMP or integrin-binding sites, or in degraded areas without significant ECM for integrin engagement. Because the focus of this study is on the role of physical ECM cues in regulating invadopodia function, and does not involve the molecular signaling scale, we decided to implement only the last concept into the model, whereby loss of ECM adhesion leads to invadopodial retraction. Although it is not clear at this point whether invadopodia mediate strong adhesion, as is thought to occur with podosomes, it is still likely that even weak adhesion to the ECM will stabilize invadopodial protrusions and prevent retraction. We used ECM degradation activity as a surrogate for adhesion to the ECM, because any productive encounter of invadopodia with ECM fibers in the model leads to fiber degradation.

We therefore modeled the retraction of invadopodia by introducing a threshold, ψ. If an invadopodium has not degraded any ECM for a certain number of consecutive time steps $\Delta t > \psi$, then it is retracted. We assumed that retraction occurred on a much smaller time scale than invadopodial protrusion, and hence the invadopodium was removed from the automaton instantaneously. With the above-discussed parameter set, a threshold for invadopodial retraction of $\psi = 15$ resulted in biologically plausible invadopodia patterns, e.g., invadopodia can still protrude, but can also be spontaneously retracted in uncross-linked ECM. In ECM domains that are cross-linked, there is an increase in retraction because of the baseline penalty that decreases degradation (and penetration) dependent on cross-linking (Fig. 6). Variation of this parameter value alters the depth of invadopodium penetration before retraction quite significantly, such that with larger ψ, invadopodia eventually protrude through all types of domains and have long lifetimes, whereas with smaller ψ, invadopodia penetrate to relatively shallow levels before retraction, and have short lifetimes (see Fig. S2 *C* in Data S1).

Figure 6 *A*, gives examples of invadopodia protruding into ECM domains with various degrees of cross-linking, as well as retractions if they have not degraded any ECM for $\psi > 15$. Similar to the results in Fig. 5, an analysis of the penetration depth of invadopodia before retraction demonstrates that the cross-linking penalty leads to decreased penetration and degradation by invadopodia in more highly cross-linked ECM domains (Fig. 6 *C*). In addition, the amount of time that an invadopodium persists before retraction is consequently decreased in highly cross-linked ECM domains (Fig. 6 *B*), because of the inability of invadopodia to progress. Interestingly, all invadopodia in the $cl = 5\%$, 10%, and 25% cross-linked domains penetrate through almost the whole domain (~1000 pixels; Fig. 6 *C*). However, invadopodia take a longer time to invade because of the increased number of cross-links and hence higher penalties in their preferred migration direction (Fig. 6 *B*). In the domains with the highest cross-linking ratios ($cl = 50\%$ and 100%), many invadopodia are retracted before they reach the bottom of the domain (Fig. 6 *A*). Thus, implementation of the retraction rule leads to a shorter lifetime for invadopodia in unfavorable ECM environments.

We also incorporated the dynamic formation of invadopodia into the model, as must occur in real life, with new invadopodia initiation occurring during the simulation with a probability of $\zeta \times 1/1500$. Under baseline conditions, $\zeta = 1$; thus, the initiation of invadopodia occurs once every 1500 time steps (Fig. 7 and Movie S2). Biologically, this baseline initiation could represent a response to intrinsic cellular signals or to growth factor signals, such as occur through EGF signaling (34). However, cells frequently modify their behavior in response to sensing the biological or mechanical properties of the surrounding microenvironment through cell-ECM adhesion. At this point, it is unclear whether an ECM that is unfavorable for degradation and penetration (e.g., highly cross-linked gelatin) would favor or diminish the initiation of new invadopodia. Therefore, we performed additional simulations in which the rate of invadopodia initiation was modified either positively or negatively by interaction with the ECM (Fig. 7).

Because invadopodial retraction occurs when an individual invadopodium is unable to degrade ECM for a specified period of time, it is an ideal readout of favorable or unfavorable ECM. Therefore, to model feedback from the ECM, we modified the initiation rate such that the frequency of initiation either increased or decreased every time an invadopodium was retracted prematurely (e.g., before it reached the bottom of the ECM domain). To be considered an invadopodium that can trigger feedback, a protrusion must at some point degrade at

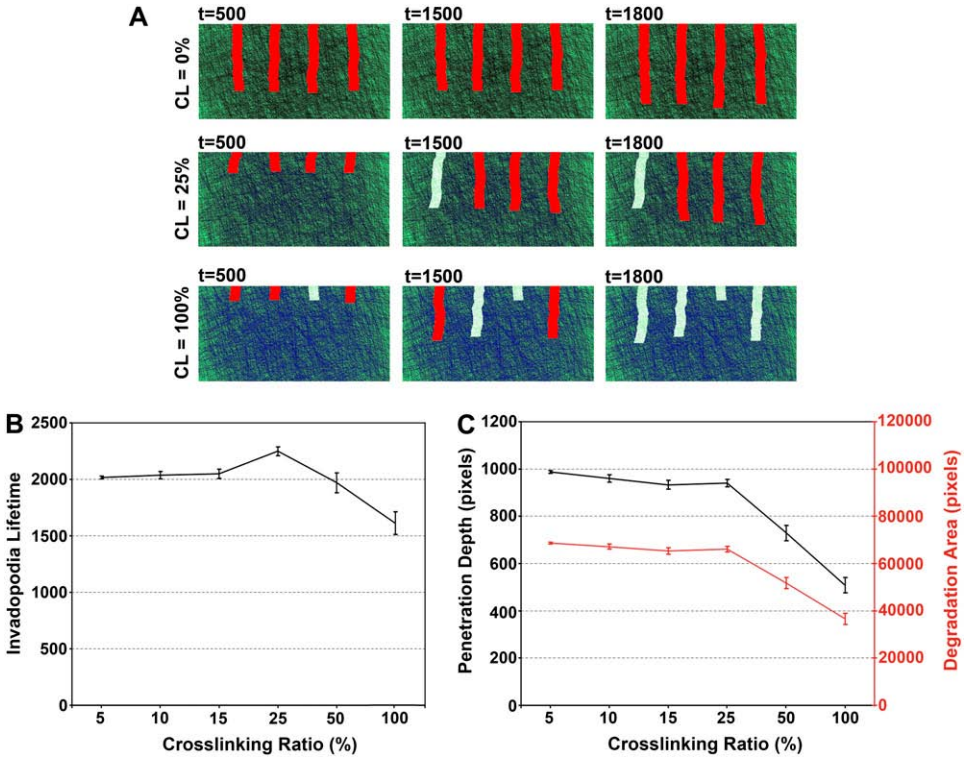

FIGURE 6 Inclusion of invadopodia retraction in the model. In these simulations, a retraction rule was implemented in which any invadopodium that does not degrade ECM for $\psi > 15$ time steps becomes retracted. Simulations were initiated with four invadopodia, and were run until all invadopodia were retracted. (*A*) Sample screen shots at various times from simulations of invadopodia going through ECM domains with 0%, 25%, or 100% cross-linking. Note that retraction (empty stripe where red invadopodium was) occurs before reaching the end of the domain in the 25% and 100% conditions, because of the immobility of invadopodia. (*B*) Graph of invadopodia lifetime (number of timesteps until retraction). In the 25% cross-linking condition, the average invadopodia lifetime increases because the majority of invadopodia reach the end of the domain without retraction, but with a delay compared to the 0%, 5%, and 10% cross-link conditions. (*C*) Invadopodia penetration depth (*black line*) and ECM degradation (*red line*) at time of retraction, with respect to cross-link ratio. Because simulations were run until no invadopodia were in the domain, penetration and degradation inhibition in cross-linked ECM occurred only when significant retraction occurred (e.g., in domains with cross-link ratios of 50% or 100%). Shown is the mean ± SE from 60 invadopodia for each cross-linking variable.

least one pixel of matrix. This latter rule was necessary to avoid large accelerations in invadopodia initiation that occasionally occur in the positive feedback simulations from transient protrusions (lamellipodia) that are initiated into empty space and retracted before ever degrading the ECM. Using a baseline initiation rate with $\zeta = 1$, an average of 6.7 invadopodia is formed over the course of the 10,000 time-step simulation. If we decrease the baseline rate of invadopodia formation by 25% every time an invadopodium is retracted ($\zeta = 0.75$), the number of invadopodia formed in the 0% cross-linked matrix decreases to 5.0. In the 100% cross-linked ECM, there is an additional 26% decrease in invadopodia number compared with uncross-linked matrices (Fig. 7). Conversely, if we increase the baseline rate of invadopodia formation by 10% ($\zeta = 1.1$) with each invadopodium retraction, the average number of invadopodia formed during 10,000 time steps increases to 7.7 in the 0%, and increases further by 28% in the 100% cross-link ratio condition.

One notable effect of the feedback rule is that there is not only an effect of cross-linking on invadopodia number, but also an overall impact on invadopodia formation in uncross-linked matrix for different values of ζ (e.g., 0.75, 1, or 1.1) (Fig. 7). This outcome derives from the use of retraction as the trigger to alter the rate of invadopodia formation, rather than directly tying the rate to ECM cross-linking (or other matrix characteristics). This provides a mechanism for self-adjustment to the matrix conditions, and amplifies the effect of single invadopodium-ECM interactions. For example, the addition of invadopodia dynamics in the form of the retraction and initiation rules amplifies the response to 100% cross-linked matrix, such that there is a greater decrease in ECM degradation with cross-linking than in simulations run without dynamics (42%, 48%, and 58% in the positive, baseline, and negative feedback conditions, respectively, in Fig. 7, compared with 30% with no dynamics, in Fig. 5). In experiments, the only measurement that we could perform on an individual invadopodium was penetration depth, which demonstrated a 26% decrease between high and low cross-linking conditions, and was purposely used to calibrate the model (30% decrease in simulated invadopodium penetration depth in Fig. 5). However, our experimental ECM degradation measurements reflect the collective activity of the entire cell, and thus likely reflect invadopodia dynamics, and exhibit a larger decrease with cross-linking, e.g., 42% and 79% decreases in functional invadopodia and ECM degradation area/cell area, respectively, when comparing 2.5% and 0.1% glutaraldehyde conditions. Thus in both the model and our experiments, the collective behavior of dynamic invadopodia amplifies the effect of cross-linking.

Experimental testing of feedback models

To test whether ECM cross-linking in real cells affects invadopodia dynamics, and to compare the results with our

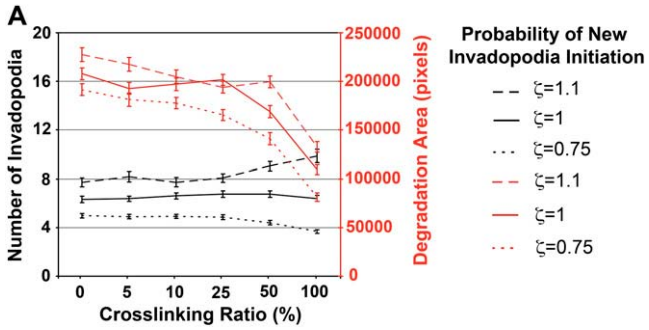

FIGURE 7 Inclusion of new invadopodia formation in the model. Formation of new invadopodia was modeled by implementing a background initiation of new invadopodia with a probability of $\zeta * 1/1500$ (once every 1500 time steps). Under baseline conditions, $\zeta = 1$. Modification of this baseline rate by invadopodia retraction led to either positive ($\zeta = 1.1$) or negative ($\zeta = 0.75$) feedback from ECM conditions. A single invadopodium was initiated at time = 0 in our standard ECM domains, to allow room for additional invadopodia that formed during the simulation. Plot shows the number of newly initiated invadopodia (*black*) and degraded ECM (*red*) as a function of ECM cross-linking and ζ, as indicated. These data were taken from simulations that were run for 10,000 time steps. Shown is the mean ± SE from 100 invadopodia for each cross-linking variable. See also Movie S2.

feedback simulation models, we performed live-cell imaging of invadopodia. We cultured CA1d cells that stably express GFP-ARPC1 (a subunit of the Arp2/3 complex that localizes to invadopodia) on Texas-red-labeled gelatin cross-linked with 0.1% or 2.5% glutaraldehyde, imaged for 2 h with a frame taken every minute. Fig. 8 shows representative images from movies that were used to quantify average lifetimes of invadopodia and numbers of invadopodia formed over time (see also Movie S3 and Movie S4). For the quantification of invadopodia dynamics in these experiments, punctate GFP-ARPC1 was considered a positive indicator of invadopodium formation. Cells cultured on gelatin treated with 0.1% glutaraldehyde developed numerous invadopodia that were long-lasting (49 ± 4 min, Fig. 8 *D*) and that degraded the ECM (data not shown). By contrast, cells cultured on 2.5% glutaraldehyde-cross-linked gelatin developed invadopodia that were shorter-lived (31 ± 2 min, Fig. 8 *D*) and that typically did not degrade the ECM (data not shown). Interestingly, cells cultured on gelatin that was treated with 2.5% glutaraldehyde developed slightly more new invadopodia per hour than cells cultured on gelatin cross-linked with 0.1% glutaraldehyde, although these results were not statistically significant (2.1 ± 0.5 compared with 1.5 ± 0.5 invadopodia per hour, for 2.5% and 0.1% glutaraldehyde-cross-linked gelatin, respectively; Fig. 8 *C*). These data suggest that a permissive ECM is necessary for the maturation of invadopodia and degradation of the ECM, and favor the model in which unsuccessful invadopodia are retracted early. The slight increase in new formation of invadopodia is consistent with our model of positive feedback from cross-linked matrices. However, further study is required to validate that finding and determine potential mechanisms.

Interaction of invadopodia with sparse collagen gels: model predictions

A current debate in the cell-motility and invadopodia field relates to whether and where proteolytic activity is required during cell movement through diverse tissues. Dense gelatin substrates, which may serve as an in vitro model for basement

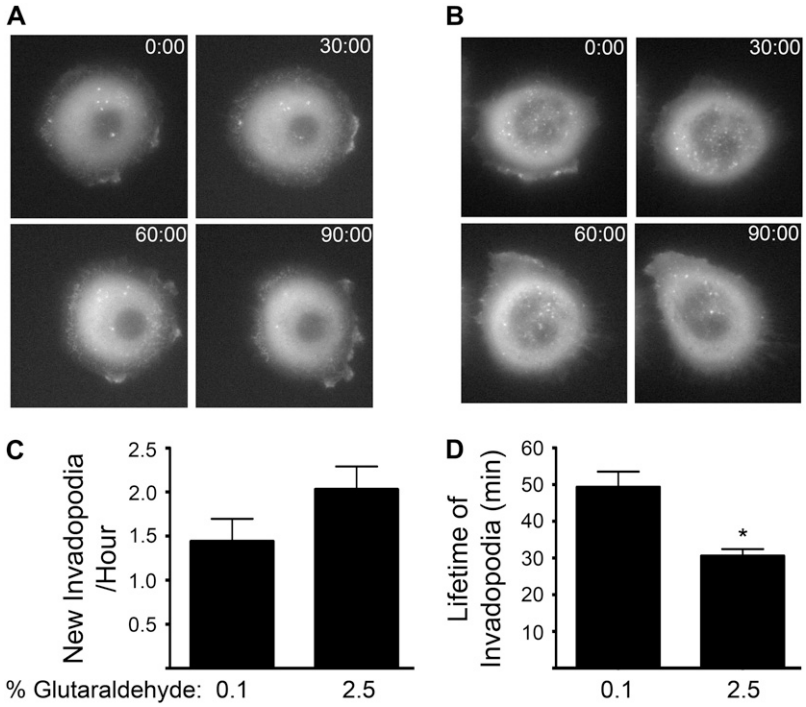

FIGURE 8 Invadopodia lifetime is regulated by ECM cross-linking. (*A*) Images from 2-h movies taken of CA1D cells expressing GFP-ARPC1 cultured on 0.1% cross-linked Texas-red gelatin. Time scale is in minutes. See also Movie S3. (*B*) Images from 2-h movies taken of CA1D cells cultured on 2.5% cross-linked Texas-red gelatin. Time scale is in minutes. Note the increased number of invadopodia over the course of the movie. See also Movie S4. (*C*) Quantification of number of newly developed invadopodia that appeared during filming of the movies. (*D*) Quantification of lifetimes of invadopodia that appeared and disappeared during filming of movies. Data for each condition are reported as mean ± SE, and are taken from six independent experiments with 25 individual cells. $*p < 0.05$.

membranes, are typically used in invadopodia experiments, whereas sparser collagen gels that are used for 3D cell-motility experiments are thought to approximate loose stromal connective tissue. For collagen gels used in 3D motility assays, the type of collagen used (e.g., Vitrogen versus rat-tail collagen) and the polymerization conditions can lead to the differential formation of thicker or thinner fibrillar structures known as macrofibrils and microfibrils, respectively, from triple-helical collagen monomers. These different structures are likely to exert a large impact on cell invasion, yet have not been systematically studied.

From the experimental standpoint, there are technical limitations to determining how diverse collagen structures affect invadopodia. The fluorescent matrix degradation assay that is used to quantitate invadopodia functions (Fig. 3) is limited by optics, in that only very thin gels ($\sim$1 μm thick) will allow the detection of ECM degradation. Thus, the typical polymerization of gels from an acid solution to form microfibrils or macrofibrils would form overly thick gels that would not allow the detection of invadopodia activity, although triple-helix collagen monomers can be coated thinly (see Fig. S3 in Data S1). Also, identifying the proportion of various species of collagen in polymerized collagen gels is difficult, because only fibrils that are above the resolution limit of the light microscope (diameter $\geq$200 nm), e.g., macrofibrils, are easily detected using techniques such as confocal reflectance microscopy and second-harmonic generation.

Because we built this model with physiologic length scales, it can be used to examine invadopodia interactions with diverse matrices. We therefore altered the computational ECM to contain different type I collagen structures: monomers (e.g., triple helices without any larger-order structure), microfibrils, and macrofibrils (Table 2 for dimensions and fiber numbers). Microfibril formation involves the staggered association of five triple-helical collagen monomers in a cylindrical arrangement, with a width of 3–5 nm and variable lengths (31). If we assume that the microfibrils do not extend beyond the domain and have a length of 300 nm, with 15 collagen α-chains per microfibril, then there are 17.6 fibers in our 1.67 mg/mL microfibril domain (Fig. 9 *A*and Table 2). This concentration was modeled for comparison with the concentrations that were used for 3D motility experiments (35,36). However, the fiber number from a pure microfibril domain represents an overestimate, because much of the collagen undergoes further association into macrofibrils, depending on the source of collagen (37). If we assume that all of the collagen associates into macrofibrils, with a diameter of 400–500 nm (37), then there must be much less than one fiber in a 1.67 mg/mL collagen ECM domain, because the diameter is 100-fold wider than a microfibril. A comparison of ECM domains with 25 mg/mL gelatin, 1 mg/mL collagen monomers, and 1.67 mg/mL microfibrils is shown in Fig. 9 *A*. For a 1.67 mg/mL concentration, there would be much less than one macrofibril per domain. However, for comparative purposes, we also show one macrofibril in our ECM domain (Fig. 9 *A*).

To examine the interaction of invadopodia with sparse collagen substrates, we initialized the model with 1 mg/mL type I collagen monomers. We used the known dimensions of triple-helical collagen monomers, i.e., 300 nm $\times$ 1.5 nm (29–32). Based on our assumption that all the fibers in the gelatin were single-stranded, the number of collagen fibers was reduced by 75-fold (25-fold decrease in mg/mL concentration $\times$ 3-fold decrease because of the formation of triple-helical monomers) compared with 25 mg/mL gelatin, such that there are only 53 fibers in the domain (Fig. 9 *A* and Table 2). Invadopodial protrusion into this 1 mg/mL collagen domain was examined under two conditions: 1), as in Fig. 5, without invadopodia dynamics (Fig. 9 *B*, *left* and *C*); and 2), as in Fig. 7, with invadopodia retraction and initiation included (Fig. 9 *B*, *right* and Fig. 9 *D*). As before, penetration and degradation of ECM in 0%, 5%, 10%, 25%, 50%, and 100% cross-link ratios were determined for either 1000 time steps (Fig. 9 *C* and Movie S5) or 10,000 time steps (Fig. 9 *D* and Movie S6). In contrast to our findings in cross-linked gelatin, both in silico and in experiments, the simulation results showed no effect of cross-linking on ECM degradation or invadopodia penetration in 1 mg/mL collagen monomer domains. This was likely because of the low number of cross-links in the sparse fiber domain, such that an invadopodium rarely interacted with cross-linked fibers. The same effect will hold true for the microfibril and macrofibril domains, which are even more sparsely populated with fibers. Thus, in sparse collagen gels, any single invadopodium will only rarely encounter a collagen fibril and degrade it (note the low fiber degradation in 1 mg/mL collagen gels compared with gelatin, Fig. 9 *C* and *D*, *red lines at bottom*). If the concentration of collagen monomers in the ECM domain is increased to 4–10 mg/mL, slight reductions in penetration and

TABLE 2 Gelatin and collagen fiber parameters

Fiber type	Concentration (mg/mL)	Number of fibers	Fiber dimensions (nm)	Fiber dimensions (pixels)
Gelatin	25	3958	0.5 $\times$ 300	1 $\times$ 600
Collagen (monomers)	25	1320	1.5 $\times$ 300	3 $\times$ 600
Collagen (monomers)	10	528	1.5 $\times$ 300	3 $\times$ 600
Collagen (monomers)	1	53	1.5 $\times$ 300	3 $\times$ 600
Collagen (microfibrils)	1.67	18	4.0 $\times$ 300	8 $\times$ 600
Collagen (microfibrils)	1	11	4.0 $\times$ 300	8 $\times$ 600
Collagen (macrofibrils)	1.67	$\ll$1	400 $\times$ variable	800 $\times$ variable

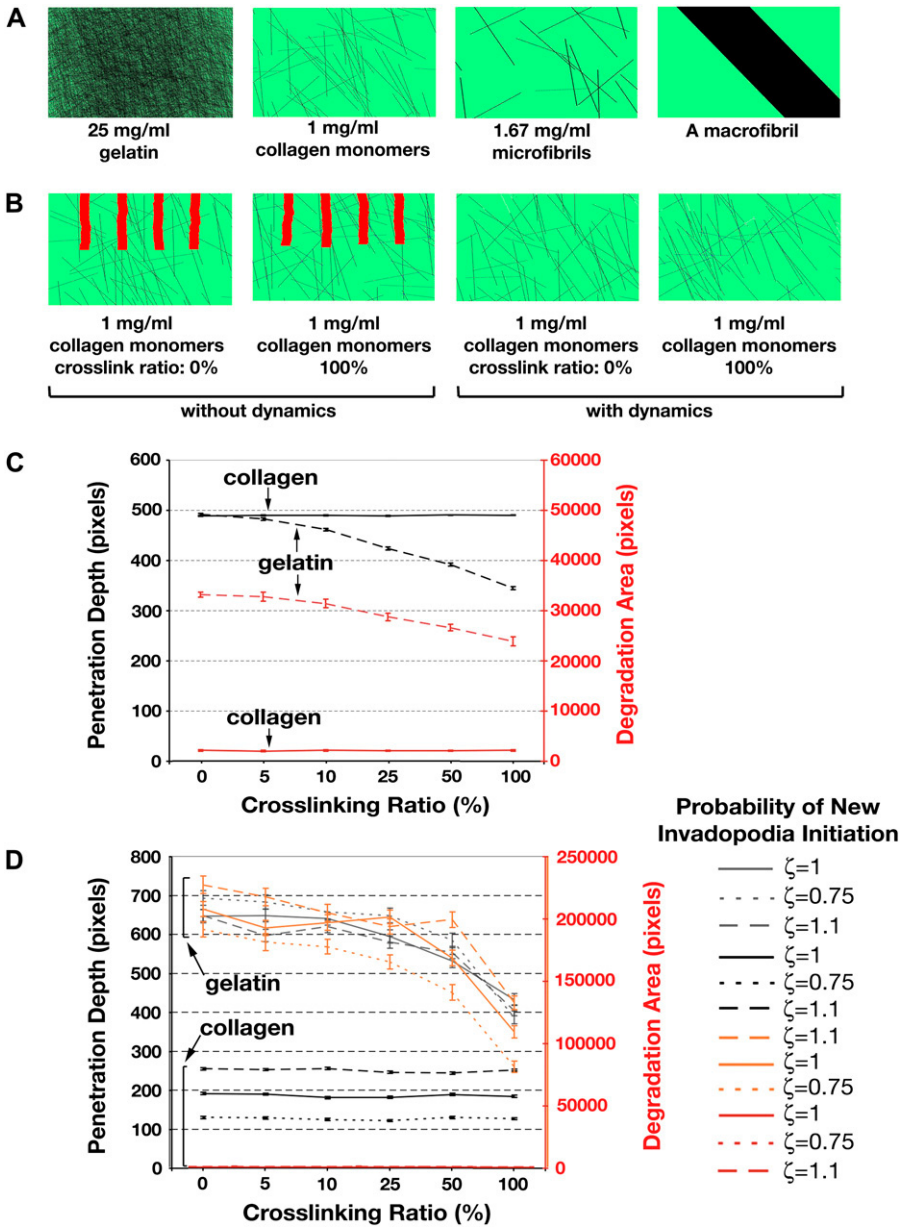

FIGURE 9 Model implementation with different ECM domains. (*A*, *left to right*) images of 25 mg/mL gelatin, 1 mg/mL collagen monomers, 1.67 mg/mL microfibrils, and a macrofibril. (*B*) Screenshots from simulations of invadopodia migrating into 0% and 100% cross-linked 1 mg/mL collagen monomers. Simulations were run with or without rules incorporating invadopodia dynamics, as indicated, for $t = 1000$ time steps (without dynamics) or $t = 10{,}000$ time steps (with dynamics). The last image from each simulation is shown. Note that with dynamics, the invadopodia are rarely present in the domain, because of a lack of interaction with ECM and rapid retraction. See also Movie S5 and Movie S6. (*C*) Plots of penetration depth (*black*) and degradation area (*red*) for 1 mg/mL collagen monomers (*solid line*) and 25 mg/mL gelatin (*dashed line*) without invadopodia dynamics. (*D*) Plots of penetration depth (*black* and *gray*) and degradation area (*red* and *orange*) for 1 mg/mL collagen monomers (*black* and *red*) and 25 mg/mL gelatin (*gray* and *orange*) with invadopodia dynamics. The ζ modifications of initiation probabilities for baseline, negative, and positive feedback are as indicated at right.

degradation are found at 5 mg/mL and above (0%, 2%, and 6% reductions in penetration and degradation with 4, 5, and 10 mg/mL collagen monomers, respectively; data not shown). Even for the 10 mg/mL collagen domain, there is a substantial decrease in fiber number compared with 25 mg/mL gelatin (Table 1), leading to far fewer cross-links and a decreased impact on penetration and degradation.

In simulations that include invadopodia dynamics, retraction occurs quickly in 1 mg/mL collagen (lifetime, on average, is ~230 time steps in any of the cross-linking conditions, compared with ~1000 time steps for gelatin in the 0% cross-linked matrices) due to lack of interaction with any matrix (Movie S6 versus Movie S2). Although this result has yet to be verified experimentally, it is known that dynamic lamellipodial protrusions that are not stabilized by adhesions are rapidly retracted (38), and it is tempting to speculate that cells migrating on or in sparse collagen gels may similarly form an increased number of nonproductive invadopodial protrusions. Indeed, protrusions with high concentrations of the invadopodia protease MT1-MMP were visualized at the leading edge of cells migrating through sparse collagen gels, and may represent such probing protrusions (36).

Experimental validation: invadopodia function on 1 mg/mL collagen substrates

To test the validity of our model results for invadopodia function in 1 mg/mL collagen substrates, we performed standard experimental invadopodia assays on 1 mg/mL type I

FITC-collagen-coated coverslips. For these experiments, coverslips were coated with a thin film of collagen monomers and cross-linked with various concentrations of glutaraldehyde. The collagen was not polymerized by changing the pH, because this would promote higher-order fibril formation and render the gels too thick for analysis of matrix degradation; the fibers should be primarily in the monomeric triple-helical form. Consistent with the model results, there was no effect of cross-linking on invadopodia penetration depth in collagen (see Fig. S3 *E* in Data S1), whereas gelatin showed a decrease (Fig. 2 *D*). In addition, as predicted by the computational model simulations, the overall FITC-collagen degradation was greatly decreased in all conditions compared with FITC-gelatin (see Fig. S3 *B* in Data S1 and Fig. 9, *C* and *D*). Contrary to model predictions, we found that the small amount of degradation in 1 mg/mL FITC-collagen was further decreased by cross-linking (see Fig. S3 *B*, *left* in Data S1). This might represent an increased sensitivity of collagen proteolysis to cross-linking, through a mechanism such as the differential location of proteolytic sites with respect to cross-links, or the differential specificity of invadopodia proteases for collagen versus gelatin.

DISCUSSION

We present evidence that ECM cross-linking inhibits invadopodia-associated degradation and penetration into the matrix, and also affects invadopodia dynamics and initiation. Our approach combined experimentation with computer modeling, to achieve a greater understanding of how ECM cross-linking affects invadopodia function under a variety of circumstances. Based on the experimental data, we designed a cellular automata model in which the dimensions and numbers of gelatin molecules and invadopodia were represented as realistically as possible, with a penalty for the invadopodia degradation of, and protrusion into, cross-linked ECM. We incorporated invadopodia dynamics into the model, and used it to test how feedback from the matrix and ECM structure affected invadopodia function. Several important new conclusions can be drawn from this study. First, cross-linking of the ECM inhibits the invadopodia-associated degradation and penetration of gelatin substrates. Second, several forms of feedback to invadopodia can occur from ECM cross-linking, such that the decreased ability to degrade heavily cross-linked ECM leads to shorter invadopodia lifetimes, but to an increased formation of new invadopodia puncta. Third, the typical cross-linked gelatin substrates used for invadopodia studies are fairly dense meshworks that can inhibit the penetration of 50-nm-wide invadopodia structures, and may approximate more closely the small pore sizes of basement membranes or hydrogels (39–41) than loose collagen gels (40,42,43). Conversely, the formation of macrofibrils in polymerized collagen gels can explain the presence of pores large enough for entire cells to squeeze through, without proteolytic activity (35,36).

To cross-link ECM substrates in vitro, we used the chemical cross-linker glutaraldehyde. However, in vivo endogenous cellular cross-linkers such as lysyl oxidase or transglutaminases act on a variety of ECM substrates (10,44), and are secreted by tumor stromal cells such as macrophages (44,45). Lysyl oxidase (LOX) is an enzyme with diverse functions outside of the cell, including ECM cross-linking, and is frequently downregulated during tumor development through multiple mechanisms, including gene methylation (16) and mutation (15). Conversely, there are reports that LOX may also promote tumor invasion because of the potential intracellular signaling mediated by LOX activity (17). Transglutaminase 2 is another extracellular enzyme known to cross-link the ECM. Relevant to our work, TG2-cross-linking was shown to inhibit the invasion of breast-cancer cells through Matrigel (8) and the turnover of ECM in endothelial-cell cultures (13), suggesting that the cross-linking-mediated inhibition of ECM degradation we describe is not an artifact of glutaraldehyde treatment. Interestingly, tumors grown in mice lacking TG2 grow faster and larger than tumors grown in normal mice, suggesting that TG2-mediated cross-linking of the ECM surrounding tumors (most likely by host inflammatory or other stromal cells) can be an important regulator of tumor size (13). Inhibition of tumor growth through TG2 cross-linking of ECM could occur through the prevention of ECM degradation and the removal of space constraints on growth by key invadopodia proteases such as MT1-MMP (46). Classic tumor invasion was also reported to be inhibited by true cross-linked basement membranes, when compared with basement membrane substrates such as Matrigel that lack significant cross-links (6). It will be interesting to learn whether diverse physiologic cross-linkers can mimic the effect on invadopodia function that we describe, using glutaraldehyde to cross-link the ECM.

Cellular automata are simple rule-based models that allow the use of general assumptions in the absence of detailed biologic data. In this study, a cellular automaton approach was chosen as an appropriate technique because of the relative dearth of biologic data on invadopodia and their interactions with the microenvironment. We did incorporate known biologic length scales into the simulations, wherever possible, and we performed modeling that was largely testable by experimental methods. However, many aspects of invadopodia function were purposely not included in the model at this initial stage. In particular, there is insufficient detail at this point to model molecular signaling networks, because that would require a knowledge of the relative importance of individual molecules and possibly of concentrations of species, depending on the modeling technique. Another aspect of microenvironment-invadopodia interactions that we did not model because of a lack of current biological data is force production, such as may occur at the invadopodia-ECM interface. This is an important future direction that will likely involve both model development and biologic experimentation, including the technical develop-

ment of experimental methods to measure forces at invadopodia.

For our initial model, we chose a minimal modeling approach, with a few assumptions based on experimental results. These assumptions include the following: invadopodia penetrate and degrade matrix simultaneously; ECM cross-linking inhibits invadopodia penetration and degradation; and fibers are linear structures, with a uniform width and length. The major factor that affected invadopodia penetration in the model was the cross-linking penalty, which was strongly affected by the number of cross-links encountered by the invadopodium at each time step. Thus, the ECM domain fiber number is a major determinant of the cross-linking penalty, because fewer fibers lead to fewer cross-links and a lower penalty. At this stage, we did not include an explicit penalty for fiber number, because preliminary experiments indicated that increasing the fiber number was not inhibitory for gelatin degradation (results not shown). We also did not include complex modes of matrix remodeling. For example, 3D migration experiments showed that ECM fibers realign after ''nicking'' (36). Such realignment would alter the spatial distribution of fibers, but is not currently accounted for in the model. However, it seems likely that future experiments and model development could allow the incorporation of additional features, such as how fiber width, number, or distribution affects degradation.

The application of these few rules led to behavior that was largely consistent with experimental results from ourselves and from the literature (6,8,13,35,36), and understandable in terms of minor differences (e.g., the small effect of cross-linking in 1 mg/mL collagen matrices). However, this model clearly represents, and was designed to be, a simplification. For example, the cross-linking penalty likely represents many contributing biological factors that are poorly understood at this point, such as any mechanical energy needed to push aside fibers, the potential inability of MMPs to access substrate cleavage sites in cross-linked ECM, and any requirement for the secretion of MMPs to allow for degradation before protrusion. In addition, we modeled gelatin as a uniform, single-stranded, linear molecule. However, gelatin is likely to be a mixture of denatured, full-length single chains in various conformations, including linear and random coils, some smaller degraded chains, and a small amount of renatured triple helices and even microfibrils (30,32). We chose not to model mixtures of conformations, because of their computational complexity and a lack of knowledge about the proportions of such molecular species in gelatin. However, future developments of this model might include a more detailed treatment of the cross-linking penalty and ECM components.

Invadopodia dynamics were modeled primarily through the retraction rule, in which unsuccessful invadopodia that do not degrade matrix for a specified number of time steps are retracted (Fig. 6). This rule assumes that a productive interaction of invadopodia with ECM will lead to degradation. Thus, prolonged nonproductive interactions with empty space or uncleavable ECM lead to instability and retraction of the protrusion. Retraction was also used as a sensor of favorable or unfavorable ECM to modify the rate of new invadopodia formation in positive or negative feedback scenarios (Fig. 7). Baseline initiation (without feedback), by contrast, occurred at a constant rate. Interestingly, the addition of invadopodia initiation and retraction to a model calibrated only with penetration depth from fixed cell analyses (Fig. 2) led to dynamic behavior that was unexpected but consistent with subsequent experimental validation, i.e., stronger effects of cross-linking on ECM degradation and retraction than on new initiation of invadopodia, regardless of feedback to invadopodia initiation.

When live-cell imaging was performed to quantitate invadopodia dynamics, there was a statistically significant decrease in the lifetime of invadopodia in cells cultured on highly cross-linked matrices (31 vs. 49 min on weakly cross-linked gelatin). There was also a nonstatistically significant increase in the number of newly formed invadopodia on highly cross-linked matrices (2.1 invadopodia per hour, compared with 1.5 on the weakly cross-linked matrix), suggesting the possible occurrence of positive feedback. Interestingly, although there could be many mechanisms (e.g., a decrease in a negative signal from degraded matrix, or an increase in integrin signaling from more rigid or merely undegraded matrices), the use of the retraction rule to model feedback to invadopodia initiation seemed to represent adequately the biologic impact of cross-linking. The model results are also consistent with our fixed-cell analyses, in which there was no difference in the number of total invadopodia, but a significant difference in the number of functional invadopodia that were associated with matrix degradation. Although at this point we cannot verify the exact nature of the feedback that leads to decreased invadopodia lifetimes on highly cross-linked matrices (e.g., retraction as opposed to failure to degrade and protrude), the simulations using retraction as a feedback rule provided a useful framework for experimental testing.

The modeling of diverse collagen structures led to several interesting findings. First, it allowed a controlled comparison between different ECM substrates, where the only differences between simulations were the numbers and widths of fibers. Comparisons of simulation and experimental results for 25 mg/mL gelatin and 1 mg/mL collagen substrates were surprisingly accurate, considering that we only calibrated the model once with penetration-depth results on cross-linked gelatin (Fig. 2). These results demonstrated that matrix density and cross-linking are two interdependent factors that play a critical role in invadopodia functions. Second, it allowed a modeling of the collagen microfibrils and macrofibrils that are formed in polymerized collagen gels used for in vitro culture studies, e.g., for 3D motility. These clearly will not impede invadopodia protrusion, and it becomes apparent that entire cells might be able to squeeze through such larger-order structures with little impedence (35), depending

on the proportion of micro- and macrofibrils and the concentrations used in the gels. The future application of this model to additional ECM substrates will be useful in understanding how ECM structure affects cellular invasiveness.

Computational models are most useful and relevant when combined with experimentation. The fusion of computation and experimentation can contribute at all stages of model development: the initial design of the model, the testing of model predictions, and model modification. However, such an interactive process is rare. We performed just such an interdisciplinary study, in which biological experimentation contributed to model development at all stages, and experiments were performed that would not otherwise have been conceived of in a typical experimental study. In the process, we gained insights into the inhibition of cellular invasiveness by cross-linked ECM, and we developed a tool for future studies. We anticipate that the iterative process of experimental testing and model development will lead to a greater understanding of how the physical microenvironment regulates cancer-cell invasiveness.

SUPPLEMENTARY MATERIAL

To view all of the supplemental files associated with this article, visit www.biophysj.org.

The authors thank the organizers of the Second Vanderbilt Integrative Cancer Biology Center (VICBC) Cancer Modeling Workshop that served as the nexus for this interdisciplinary project. This work was conducted in part using the resources of the Advanced Computing Center for Research and Education (ACCRE) at Vanderbilt University (Nashville, TN). Thanks go to Julie Maier for help with data analysis. H.E., N.R.A., L.E., C.C., J.J., N.L., M.H.Z., and A.M.W. contributed to the original model development at the VICBC Workshop, July 2006. Refined model development, simulation, and coding were designed by H.E. N.R.A. performed all experiments, with the exception of electron microscopy, and contributed intellectually to model development throughout the process. E.C. performed the electron microscopy depicted in Fig. 1. S.A.G. and N.R.A. performed the rheometry of gelatin substrates at Oak Ridge National Laboratory (Oak Ridge, TN). K.M.B. created the GFP-ARPC1-expressing CA1d cell line for live-cell imaging, and performed data analysis. A.R.A. provided mathematical modeling guidance during post-workshop development of the model. M.Z. provided critical intellectual input to the article. A.M.W. was the primary mentor for both the experimental work and the iterative process of model refinement. H.E., N.R.A., and A.M.W. cowrote the article, with input from the coauthors.

Funding was provided by National Cancer Institute grant U54CA113007 to the VICBC, and by National Cancer Institute grant K22 CA109590 to A.M.W. H.E. was supported by National Aeronautics and Space Administration Specialized Center of Research grant NNJ04HJ12G. N.R.A. was funded by National Cancer Institute training grant T32 CA09592. S.A.G. was supported by Vanderbilt School of Engineering Development Funds. Electron microscopy was performed in conjunction with the Vanderbilt University Medical Center Research Electron Microscopy Resource, which is partially supported by National Institutes of Health grants CA-68485, DK-20593, and DK-58404.

REFERENCES

1. Linder, S. 2007. The matrix corroded: podosomes and invadopodia in extracellular matrix degradation. *Trends Cell Biol.* 17:107–117.
2. Weaver, A. M. 2006. Invadopodia: specialized cell structures for cancer invasion. *Clin. Exp. Metastasis.* 23:97–105.
3. Artym, V. V., Y. Zhang, F. Seillier-Moiseiwitsch, K. M. Yamada, and S. C. Mueller. 2006. Dynamic interactions of cortactin and membrane type 1 matrix metalloproteinase at invadopodia: defining the stages of invadopodia formation and function. *Cancer Res.* 66:3034–3043.
4. Clark, E. S., A. S. Whigham, W. G. Yarbrough, and A. M. Weaver. 2007. Cortactin is an essential regulator of matrix metalloproteinase secretion and extracellular matrix degradation in invadopodia. *Cancer Res.* 67:4227–4235.
5. Burgstaller, G., and M. Gimona. 2005. Podosome-mediated matrix resorption and cell motility in vascular smooth muscle cells. *Am. J. Physiol. Heart Circ. Physiol.* 288:H3001–H3005.
6. Hotary, K., X. Y. Li, E. Allen, S. L. Stevens, and S. J. Weiss. 2006. A cancer cell metalloprotease triad regulates the basement membrane transmigration program. *Genes Dev.* 20:2673–2686.
7. Kalluri, R. 2003. Basement membranes: structure, assembly and role in tumour angiogenesis. *Nat. Rev. Cancer.* 3:422–433.
8. Mangala, L. S., B. Arun, A. A. Sahin, and K. Mehta. 2005. Tissue transglutaminase-induced alterations in extracellular matrix inhibit tumor invasion. *Mol. Cancer.* 4:33.
9. Even-Ram, S., and K. M. Yamada. 2005. Cell migration in 3D matrix. *Curr. Opin. Cell Biol.* 17:524–532.
10. Facchiano, F., A. Facchiano, and A. M. Facchiano. 2006. The role of transglutaminase-2 and its substrates in human diseases. *Front. Biosci.* 11:1758–1773.
11. Kotsakis, P., and M. Griffin. 2007. Tissue transglutaminase in tumour progression: friend or foe? *Amino Acids.* 33:373–384.
12. Smith-Mungo, L. I., and H. M. Kagan. 1998. Lysyl oxidase: properties, regulation and multiple functions in biology. *Matrix Biol.* 16:387–398.
13. Jones, R. A., P. Kotsakis, T. S. Johnson, D. Y. Chau, S. Ali, G. Melino, and M. Griffin. 2006. Matrix changes induced by transglutaminase 2 lead to inhibition of angiogenesis and tumor growth. *Cell Death Differ.* 13:1442–1453.
14. Xu, L., S. Begum, J. D. Hearn, and R. O. Hynes. 2006. GPR56, an atypical G protein-coupled receptor, binds tissue transglutaminase, TG2, and inhibits melanoma tumor growth and metastasis. *Proc. Natl. Acad. Sci. USA.* 103:9023–9028.
15. Csiszar, K., S. F. Fong, A. Ujfalusi, S. A. Krawetz, E. P. Salvati, J. W. Mackenzie, and C. D. Boyd. 2002. Somatic mutations of the lysyl oxidase gene on chromosome 5q23.1 in colorectal tumors. *Int. J. Cancer.* 97:636–642.
16. Kaneda, A., K. Wakazono, T. Tsukamoto, N. Watanabe, Y. Yagi, M. Tatematsu, M. Kaminishi, T. Sugimura, and T. Ushijima. 2004. Lysyl oxidase is a tumor suppressor gene inactivated by methylation and loss of heterozygosity in human gastric cancers. *Cancer Res.* 64:6410–6415.
17. Payne, S. L., M. J. Hendrix, and D. A. Kirschmann. 2007. Paradoxical roles for lysyl oxidases in cancer—a prospect. *J. Cell. Biochem.* 101: 1338–1354.
18. Satpathy, M., L. Cao, R. Pincheira, R. Emerson, R. Bigsby, H. Nakshatri, and D. Matei. 2007. Enhanced peritoneal ovarian tumor dissemination by tissue transglutaminase. *Cancer Res.* 67:7194–7202.
19. Yuan, L., M. Siegel, K. Choi, C. Khosla, C. R. Miller, E. N. Jackson, D. Piwnica-Worms, and K. M. Rich. 2007. Transglutaminase 2 inhibitor, KCC009, disrupts fibronectin assembly in the extracellular matrix and sensitizes orthotopic glioblastomas to chemotherapy. *Oncogene.* 26: 2563–2573.
20. DiMilla, P. A., K. Barbee, and D. A. Lauffenburger. 1991. Mathematical model for the effects of adhesion and mechanics on cell migration speed. *Biophys. J.* 60:15–37.
21. Gracheva, M. E., and H. G. Othmer. 2004. A continuum model of motility in ameboid cells. *Bull. Math. Biol.* 66:167–193.
22. Rubinstein, B., K. Jacobson, and A. Mogilner. 2005. Multiscale two-dimensional modeling of a motile simple-shaped cell. *SIAM J. Multiscale Model. Simul.* 3:413–439.

23. Zaman, M. H., R. D. Kamm, P. Matsudaira, and D. A. Lauffenburger. 2005. Computational model for cell migration in three-dimensional matrices. *Biophys. J.* 89:1389–1397.

24. Santner, S. J., P. J. Dawson, L. Tait, H. D. Soule, J. Eliason, A. N. Mohamed, S. R. Wolman, G. H. Heppner, and F. R. Miller. 2001. Malignant MCF10CA1 cell lines derived from premalignant human breast epithelial MCF10AT cells. *Breast Cancer Res. Treat.* 65:101–110.

25. Bowden, E. T., P. J. Coopman, and S. C. Mueller. 2001. Invadopodia: unique methods for measurement of extracellular matrix degradation in vitro. *Methods Cell Biol.* 63:613–627.

26. Ireton, R. C., M. A. Davis, J. van Hengel, D. J. Mariner, K. Barnes, M. A. Thoreson, P. Z. Anastasiadis, L. Matrisian, L. M. Bundy, L. Sealy, B. Gilbert, F. van Roy, and A. B. Reynolds. 2002. A novel role for p120 catenin in E-cadherin function. *J. Cell Biol.* 159:465–476.

27. Martucci, J. F., R. A. Ruseckaite, and A. Vazquez. 2006. Creep of glutaraldehyde-crosslinked gelatin films. *Mat Sci Engineer.* 435–6: 681–686.

28. Bowden, E. T., M. Barth, D. Thomas, R. I. Glazer, and S. C. Mueller. 1999. An invasion-related complex of cortactin, paxillin and PKCmu associates with invadopodia at sites of extracellular matrix degradation. *Oncogene.* 18:4440–4449.

29. Boedtker, H., and P. Doty. 1955. On the nature of the structural element of collagen. *Nature.* 77:248–249.

30. Boedtker, H., and P. Doty. 1956. The native and denatured states of soluble collagen. *J. Am. Chem. Soc.* 78:4267–4280.

31. Smith, J. W. 1968. Molecular pattern in native collagen. *Nature.* 219: 157–158.

32. Veis, A., and J. Cohen. 1960. Reversible transformation of gelatin to the collagen structure. *Nature.* 186:720–721.

33. Baldassarre, M., I. Ayala, G. Beznoussenko, G. Giacchetti, L. M. Machesky, A. Luini, and R. Buccione. 2006. Actin dynamics at sites of extracellular matrix degradation. *Eur. J. Cell Biol.* 85:1217–1231.

34. Yamaguchi, H., M. Lorenz, S. Kempiak, C. Sarmiento, S. Coniglio, M. Symons, J. Segall, R. Eddy, H. Miki, T. Takenawa, and J. Condeelis. 2005. Molecular mechanisms of invadopodium formation: the role of the N-WASP-Arp2/3 complex pathway and cofilin. *J. Cell Biol.* 168: 441–452.

35. Wolf, K., I. Mazo, H. Leung, K. Engelke, U. H. von Andrian, E. I. Deryugina, A. Y. Strongin, E. B. Brocker, and P. Friedl. 2003. Compensation mechanism in tumor cell migration: mesenchymal-amoeboid transition after blocking of pericellular proteolysis. *J. Cell Biol.* 160:267–277.

36. Wolf, K., Y. I. Wu, Y. Liu, J. Geiger, E. Tam, C. Overall, M. S. Stack, and P. Friedl. 2007. Multi-step pericellular proteolysis controls the transition from individual to collective cancer cell invasion. *Nat. Cell Biol.* 9:893–904.

37. Roeder, B. A., K. Kokini, J. E. Sturgis, J. P. Robinson, and S. L. Voytik-Harbin. 2002. Tensile mechanical properties of three-dimensional type I collagen extracellular matrices with varied microstructure. *J. Biomech. Eng.* 124:214–222.

38. Borm, B., R. P. Requardt, V. Herzog, and G. Kirfel. 2005. Membrane ruffles in cell migration: indicators of inefficient lamellipodia adhesion and compartments of actin filament reorganization. *Exp. Cell Res.* 302:83–95.

39. Abrams, G. A., C. J. Murphy, Z. Y. Wang, P. F. Nealey, and D. E. Bjorling. 2003. Ultrastructural basement membrane topography of the bladder epithelium. *Urol. Res.* 31:341–346.

40. Raeber, G. P., M. P. Lutolf, and J. A. Hubbell. 2005. Molecularly engineered PEG hydrogels: a novel model system for proteolytically mediated cell migration. *Biophys. J.* 89:1374–1388.

41. Yamasaki, Y., H. Makino, and Z. Ota. 1994. Meshwork structures in bovine glomerular and tubular basement membrane as revealed by ultra-high-resolution scanning electron microscopy. *Nephron.* 66: 189–199.

42. Raub, C. B., J. Unruh, V. Suresh, T. Krasieva, T. Lindmo, E. Gratton, B. J. Tromberg, and S. C. George. 2008. Image correlation spectroscopy of multiphoton images correlates with collagen mechanical properties. *Biophys. J.* 94:2361–2373.

43. Saltzman, W. M., M. L. Radomsky, K. J. Whaley, and R. A. Cone. 1994. Antibody diffusion in human cervical mucus. *Biophys. J.* 66: 508–515.

44. Kagan, H. M., and W. Li. 2003. Lysyl oxidase: properties, specificity, and biological roles inside and outside of the cell. *J. Cell. Biochem.* 88:660–672.

45. Fesus, L., and M. Piacentini. 2002. Transglutaminase 2: an enigmatic enzyme with diverse functions. *Trends Biochem. Sci.* 27:534–539.

46. Hotary, K. B., E. D. Allen, P. C. Brooks, N. S. Datta, M. W. Long, and S. J. Weiss. 2003. Membrane type I matrix metalloproteinase usurps tumor growth control imposed by the three-dimensional extracellular matrix. *Cell.* 114:33–45.